



OPEN

SUBJECT AREAS:

OPTICAL SENSORS

OPTOELECTRONIC DEVICES AND  
COMPONENTS

INTEGRATED OPTICS

Received  
5 November 2013Accepted  
14 April 2014Published  
6 May 2014Correspondence and  
requests for materials  
should be addressed to  
H.Q.L. (lihongqiang@  
tjpu.edu.cn)

# Preliminary Investigation of an SOI-based Arrayed Waveguide Grating Demodulation Integration Microsystem

Hongqiang Li<sup>1</sup>, Wenqian Zhou<sup>1</sup>, Yu Liu<sup>1</sup>, Xiaye Dong<sup>1</sup>, Cheng Zhang<sup>1</sup>, Changyun Miao<sup>1</sup>, Meiling Zhang<sup>1</sup>, Enbang Li<sup>1,2</sup> & Chunxiao Tang<sup>1</sup><sup>1</sup>School of Electronics and Information Engineering, Tianjin Polytechnic University, Tianjin 300387, China, <sup>2</sup>School of Physics, Faculty of Engineering and Information Sciences, University of Wollongong, Wollongong, NSW 2522, Australia.

An arrayed waveguide grating (AWG) demodulation integration microsystem is investigated in this study. The system consists of a C-band on-chip LED, a  $2 \times 2$  silicon nanowire-based coupler, a fiber Bragg grating (FBG) array, a  $1 \times 8$  AWG, and a photoelectric detector array. The coupler and AWG are made from silicon-on-insulator wafers using electron beam exposure and response-coupled plasma technology. Experimental results show that the excess loss in the MMI coupler with a footprint of  $6 \times 100 \mu\text{m}^2$  is 0.5423 dB. The  $1 \times 8$  AWG with a footprint of  $267 \times 381 \mu\text{m}^2$  and a waveguide width of  $0.4 \mu\text{m}$  exhibits a central channel loss of  $-3.18$  dB, insertion loss non-uniformity of  $-1.34$  dB, and crosstalk level of  $-23.1$  dB. The entire system is preliminarily tested. Wavelength measurement precision is observed to reach  $0.001$  nm. The wavelength sensitivity of each FBG is between  $0.04$  and  $0.06$  nm/dB.

Fiber Bragg grating (FBG) sensors are one of the most exciting developments in the fields of fiber-optic sensors in recent years<sup>1</sup>, while the large footprint and high price of FBG demodulation systems limit the popularization and application of optical FBG sensing technology<sup>2,3</sup>. Arrayed waveguide grating demodulation methods, which have high precision and fast demodulation, are a potential type of FBG demodulation method, and some relevant studies have been reported<sup>4,5</sup>. The heterogeneous integration of a light source<sup>6,7</sup>, an optical coupler, an AWG, and a photoelectric detector (PD) give the arrayed waveguide grating demodulation integration microsystem a compact structure, device integration, a low cost, and improved stability and reliability for the optical path. This invention is utilized to simulate optical FBG sensor demodulation and plays an important role in research on silicon optoelectronic integrated chips.

An arrayed waveguide grating demodulation integration microsystem is fabricated and tested in this study. The system consists of a C-band on-chip LED, an input grating coupler, a  $2 \times 2$  silicon-nanowire-based coupler, an FBG array, a  $1 \times 8$  AWG, an output grating couplers, and a PD array. The coupler and AWG are made from silicon-on-insulator (SOI) wafers using electron beam exposure and response-coupled plasma technology<sup>8,9</sup>. The C-band on-chip LED and PD are made from InP-based materials<sup>10,11</sup>. Light enters the coupler's input waveguide and then enters the FBG array through the grating. The reflected light enters the AWG through the coupler. The light from the AWG's output waveguides enters the InGaAs-based PD array through the gratings. The InP-based LED and photodetectors are bonded to the SOI wafer using BCB glue. The optical signals from the AWG's output waveguides are converted into electrical signals by the PD array. These electrical signals are sent to the signal processing unit for processing after amplification and A/D conversion. We designed the InP-based C-band on-chip LED, PD array, silicon-nanowire-based  $2 \times 2$  couplers, and  $1 \times 8$  AWG. The fabricated microsystem has a compact structure, device integration, low cost, precision, and rapid demodulation, thereby improving the stability of the optical path and reliability.

## Results

The arrayed waveguide grating demodulation integration microsystem is shown in Figure 1. The entire system is preliminarily tested after testing each individual device. Light from the C-band on-chip LED first enters the coupler's input waveguide and then enters the FBG array through the grating. The reflected light then enters the AWG through the coupler.

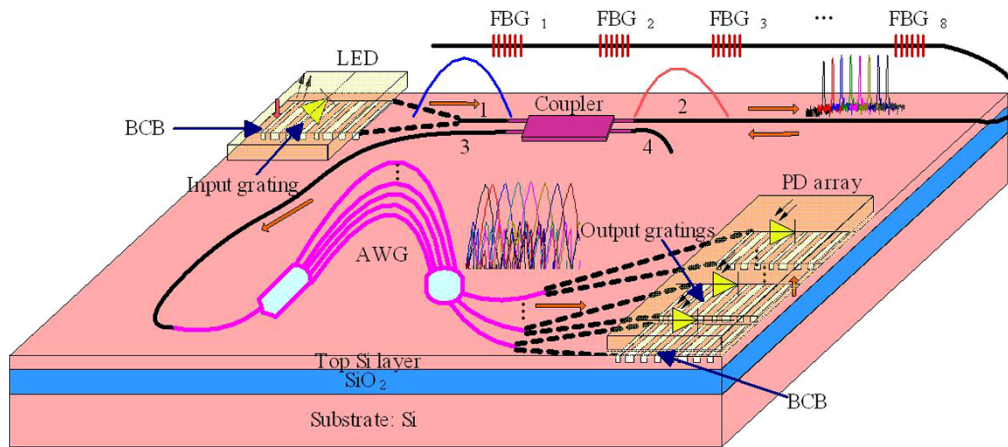


**Figure 1** | Arrayed waveguide grating demodulation integration microsystem.

The basic structure of the InP-based C-band on-chip LED is as follows. Above the InP substrate are the n-InP buffer layer, the InGaAsP active layer, the p-InP limiting layer, and the p-InGaAsP top layer, which have thicknesses of 0.5, 0.1, 0.5, and 0.5  $\mu\text{m}$ , respectively. The footprint of the InP-based C-band on-chip LED is  $360 \times 360 \mu\text{m}^2$ . At a forward bias voltage of 0.8 V, the peak wavelength of the LED's output spectrum is 1550 nm, the maximum positive bias current is 100 mA, the luminous power is  $8.1 \mu\text{W}/\mu\text{m}^2$ , and the 3 dB bandwidth is greater than 100 nm. The output spectrum of the LED is shown in Figure 2.

The light from the LED irradiates vertically to the grating coupler and diffracts into the  $2 \times 2$  coupler's input waveguide. The grating is etched on an SOI wafer. Between the grating coupler and the  $2 \times 2$  coupler's input waveguide is a tapered waveguide. A binary blazed grating is employed to achieve high coupling efficiency and a good extinction ratio. The proposed structure has a multilayered configuration. A thin grating layer is etched on the topmost silicon waveguide of the SOI wafer. To achieve high performance, a number of designed parameters should be considered, including the angle of incidence  $\theta$ , the grating period  $T$ , the number of sub-cycles in one cycle  $m$ , the duty cycle  $f_i$  ( $i = 1, 2, 3, 4$ ), the groove depth  $t_g$ , and the thickness of the top Si layer  $t_w$ . A grating coupler model is established based on the above parameters, and a simulation of the grating coupler is performed using a finite-difference time-domain (FDTD) algorithm. The binary blazed grating scheme and the experimental result with optical field of the designed grating are shown in Figure 3(a) and

3(b). The duty cycles of the blazed grating  $f_i$  ( $i = 1, 2, 3, 4$ ) are 0.348, 0.497, 0.519, and 0.652. We also obtained values of  $T = 2.296 \mu\text{m}$ ,  $m = 4$ ,  $t_g = 0.07 \mu\text{m}$ , and  $t_w = 0.22 \mu\text{m}$  when  $\theta = 0^\circ$ . This coupler has dimensions of  $360 \times 360 \mu\text{m}^2$ . The simulated coupling efficiency is 59% with vertical light irradiation, and the experimental result is 40.9% with 3 dB bandwidth of 69 nm (from 1519 nm to 1588 nm).

The light from the AWG's output waveguides enters the InGaAs-based PD array through the gratings. It is a polarization-independent grating coupler that couples SOI nanophotonic waveguides with photodetectors for silica-based hybrid integrated photodetectors. This coupler has good coupling bandwidth, high coupling efficiency, and dimensions of  $53 \times 53 \mu\text{m}^2$ . The optical field of the output grating and the experimental result are shown in Figure 3(c). The experimental result reaches 56% from 1532 nm to 1589 nm. The etching depth and the cycle are 0.07 and 0.707  $\mu\text{m}$ , respectively, and the duty ratio is 0.7.

The compact silicon nanowire-based  $2 \times 2$  MMI coupler is fabricated and tested. A tunable laser and a polarizing beam splitter (PBS) are utilized on the C-band during testing. The excess loss of the PBS is approximately 0.0560 dB. The power of the TM output port is 0.55 dB less than that of the TE output port, according to the experimental results. SMF-28 with a tapered tip at one end is utilized to couple the light source and chips. The footprint of the MMI region is only  $6 \times 57 \mu\text{m}^2$ . Theoretically, the excess loss of the MMI coupler is 0.46 dB. Experimentally, the loss is 0.5423 dB. The maximum excess loss is 1.55 dB, which is in the wavelength range of 1490.0 nm to 1590.0 nm. The experimental non-uniformity of the MMI coupler is 0.0063 dB when the center wavelength is 1550.0 nm. The maximum excess loss of the MMI coupler is 0.8233 dB when the wavelength range is 1500.0 nm to 1600.0 nm. The excess loss is defined as follows:

$$EL = -10 \lg \frac{\sum P_{OUTi}}{P_{IN}} \text{ (dB)} \quad (1)$$

The micrograph and output spectrum of the MMI coupler when the center wavelength ranges from 1500.0 nm to 1600 nm are shown in Figure 4(a), where 1TE represents the output spectrum of the coupler's bar path in TE mode, 1TM represents the output spectrum of the coupler's bar path in TM mode, 2TE represents the output spectrum of the coupler's cross path in TE mode, and 2TM represents the output spectrum of the coupler's cross path in TM mode. The polarization-dependent loss of the bar path is 3.5790 dBm, and that of the cross path is 5.3040 dBm. The experimental results show that a small  $2 \times 2$  MMI coupler that is suitable for optoelectronic integration exhibits low excess loss, wide bandwidth, and good uniformity.

The footprint of the designed AWG is  $267 \times 381 \mu\text{m}^2$ ,  $\Delta L = 19.7 \mu\text{m}$ ,  $f = 67 \mu\text{m}$ , and  $FSR = 55390 \text{ nm}$ . The simulation results

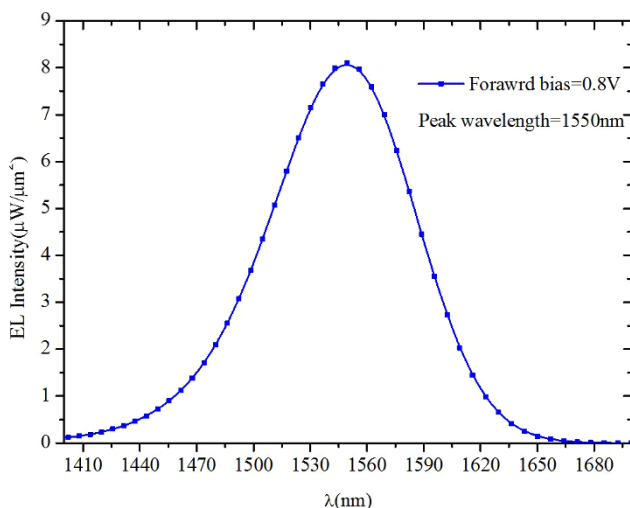


**Figure 2** | Output spectrum of the LED.

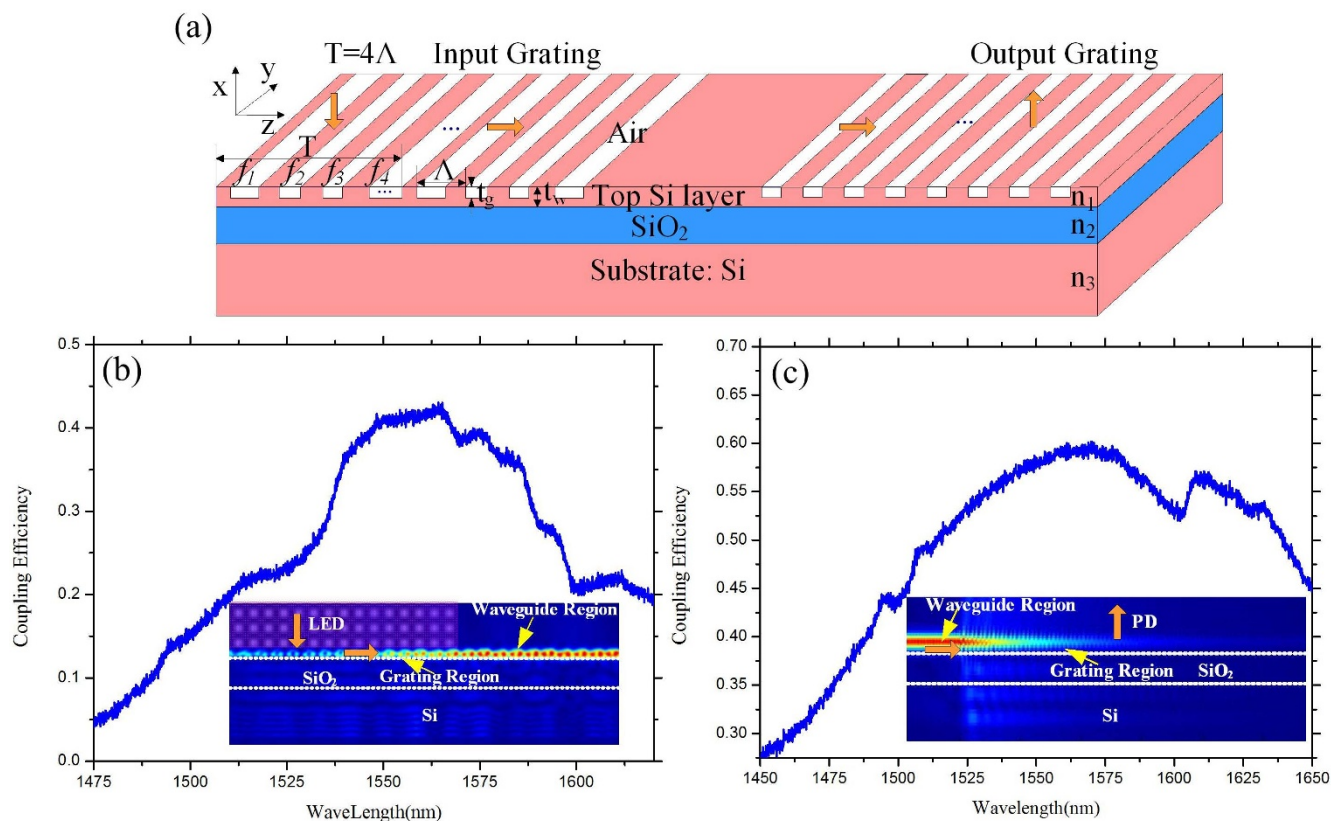


**Figure 3** | Structure and experimental results with optical field of SOI-based grating. (a) The structure of the input and output gratings. (b) and (c) The input and output experimental results with optical fields of the grating couplers, respectively.

show that the insertion loss of the AWG is 3.15 dB and that the crosstalk is 25.5 dB, which is low considering that the waveguide, thickness, and size are similar. The center wavelengths of the output channel are 1542.7, 1544.6, 1546.1, 1548.0, 1550.0, 1552.8, 1554.9, and 1556.7 nm. The channel spacing is 2.526 nm. The AWG was tested separately without the FBGs' reflection, and the output spectrum of the discrete  $1 \times 8$  AWG is shown in Figure 4(b). The center wavelengths of the output channel are 1543.9, 1545.1, 1544.7, 1549.0, 1551.0, 1553.1, 1555.0, and 1557.1 nm. The  $1 \times 8$  AWG with a waveguide width of  $0.4 \mu\text{m}$  exhibits a central channel loss of  $-2.15$  dB, an insertion loss non-uniformity of 0.8 dB, and a crosstalk level of  $-25.5$  dB in the simulation. A central channel loss of  $-3.18$  dB, an insertion loss non-uniformity of  $-1.35$  dB, and a crosstalk of  $-19.7$  dB, as defined by the phase error and adjacent channel crosstalk level, are achieved in the experiment. The spots of the output channels are clear and uniform. The value of 1 dB bandwidth of the AWG channels are 0.482, 0.472, 0.475, 0.49, 0.481, 0.416, 0.452, and 0.446 nm, the value of 3 dB bandwidth of the AWG channels are 0.775, 0.813, 0.802, 0.79, 0.821, 0.791, 0.821, and 0.815 nm. The non-uniformity of the 1 and 3 dB bandwidths are 0.074 and 0.046 nm, respectively.

The structure of the InGaAs/InP type PIN photodetector is described as follows. Three layers, i.e., an n-InP buffer layer, an i-InGaAs intrinsic absorption layer, and a p-InP layer, exist above the InP substrate, which thicknesses of 1, 3, and  $1 \mu\text{m}$ , respectively. The structure of the electrode and the thickness of the intrinsic absorption layer are improved and optimized to eliminate harmful electrode optical absorption and meet the phase matching condition of coupling. The PD is simulated using Silvaco. The PD is fabricated through heterogeneous integration technology with silicon and III-V materials. Light from the AWG's output waveguide couples with the PD array via the grating. The advantage of this coupling method is that a thick BCB glue layer can be utilized. The footprint of the PD is  $460 \times$

$170 \mu\text{m}^2$ , the dark current is less than 0.5 nA at a reverse bias of 5 V, the sensitivity is approximately 3 nW, and the photosensitive area is  $75 \times 75 \mu\text{m}^2$ .

The peak value of the FBGs' reflection spectrum is approximately  $-40.43$  dBm. The reflectivity of each FBG is approximately 90.16%, and the full width at half maximum is approximately 0.22 nm. When temperature is maintained at  $20^\circ\text{C}$ , the center wavelengths of the FBGs' reflection spectrum are 1543.01, 1545.02, 1546.98, 1549.01, 1550.99, 1553.02, 1555.03, and 1557.01 nm, according to the experimental results, as shown in Figure 4(c).

Before the PD array is bonded to the SOI wafer, we first tested the output spectrum of the  $1 \times 8$  AWG using optical spectrum analyzers. The experimental environment and photos of the main devices on the SOI chip are shown in Figure 5. An auto-align system and optical waveguide alignment are used during testing. An LCD was connected to observe the devices on the SOI chip. Figure 4(d) shows the spectrum of the  $1 \times 8$  AWG with the FBGs' reflection. The extinction ratio between the channels was considerably different from the discrete AWG because of the FBGs' influence. The AWG's two adjacent channels were inserted into the optical power meter, and the temperature changed from  $20^\circ\text{C}$  to  $50^\circ\text{C}$ . The experiment was repeated twice. Figure 6 shows the demodulation experiment result and the linear fit curve. The wavelength measurement precision of the system is 0.001 nm. The wavelength sensitivity of each FBG is between 0.04 and 0.06 nm/dB.

## Discussion

For the microsystem, the measurement of the temperature response is significant. In our study, before the PD array is bonded to the SOI wafer, an FBG with a central wavelength of 1550.99 nm at  $25^\circ\text{C}$  is selected, and the AWG  $i$  and  $i + 1$  channels are used as the output channels during demodulation. The central wavelength of the  $i$  channel is 1551.739 nm at  $25^\circ\text{C}$ , and the central wavelength of the  $i + 1$

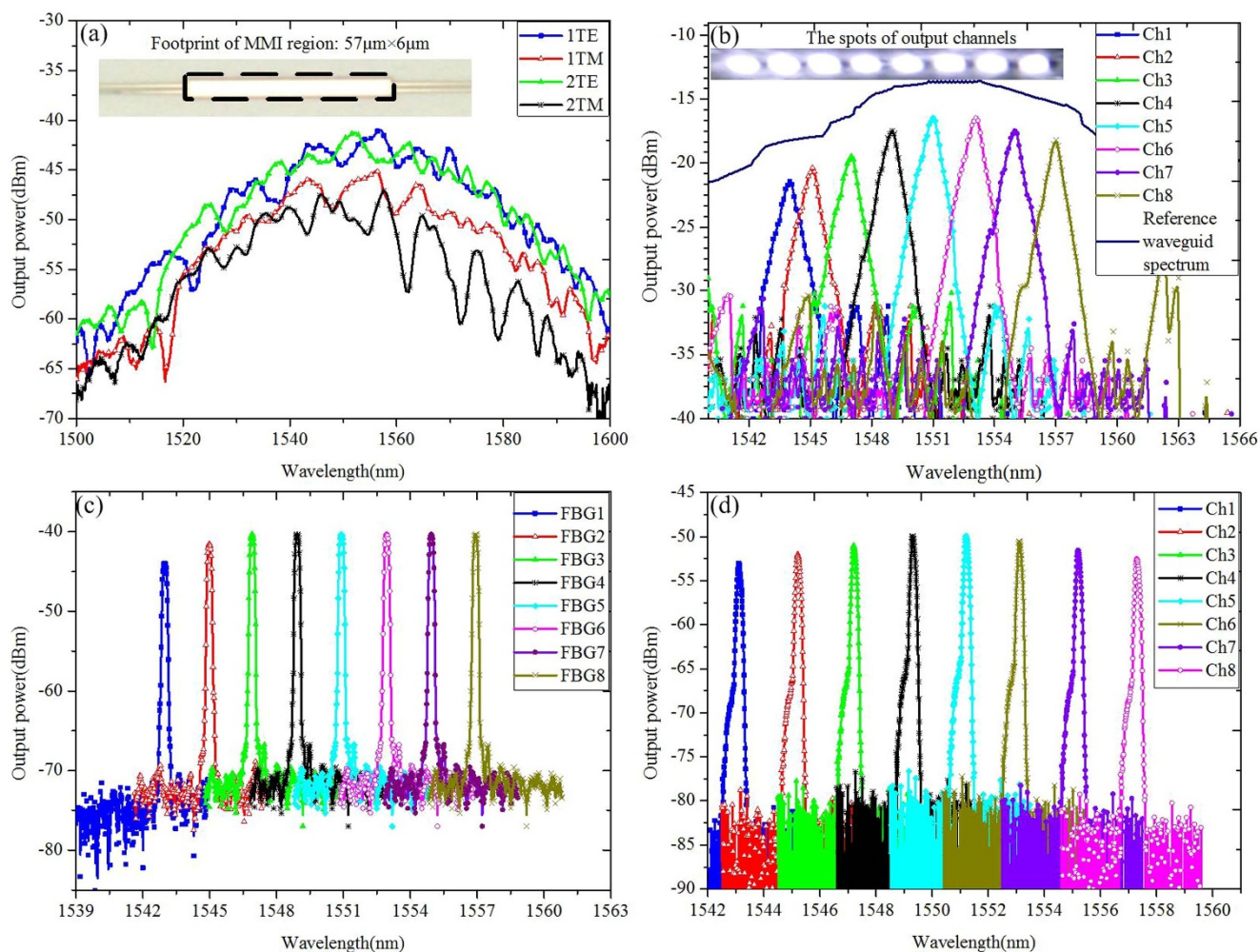


**Figure 4** | The experimental results of the microsystem. (a) The micrograph and output spectrum of the MMI coupler when  $w = 6 \mu\text{m}$ . (b) The output spectrum of the discrete  $1 \times 8$  AWG. (c) The reflection spectrum of the FBGs. (d) The spectrum of the light reflected by the FBG that enters the  $1 \times 8$  AWG through the coupler.

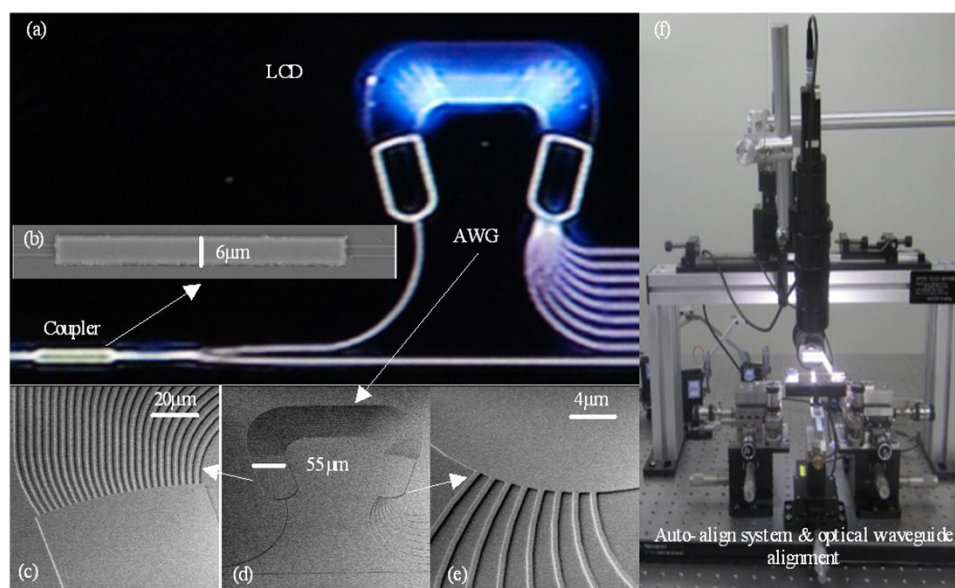


**Figure 5** | The experimental environment. (a) Main devices on the SOI chip displayed by an LCD screen. (b) SEM micrograph of the designed MMI coupler. (c), (d), and (e) SEM micrographs of the designed AWG. (f) Auto-align system and optical waveguide alignment.

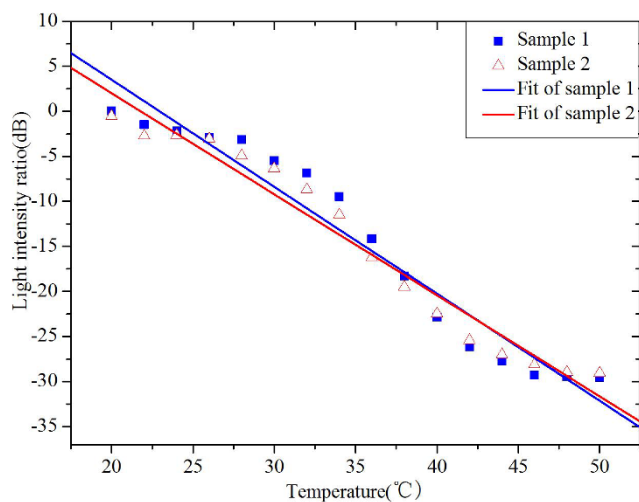


**Figure 6** | The curve fit of the relationship between the light intensity ratio and temperature.

channel is 1550.935 nm at 25°C. FBGs are placed in the water bath, with the temperature changing from 20°C to 50°C. The output light from the light source penetrates the FBG through the coupler. The reflected light also penetrates the AWG through the coupler. The AWG  $i$  and  $i + 1$  channels are inserted into the optical power meter. AWG is subjected to a constant temperature in an experiment box. Each FBG was carefully chosen to ensure that the central wavelength is between the central wavelengths of two certain AWG adjacent channels; therefore, there is no influence on the other AWG channels. In distributed measurements, the FBGs with different wavelengths are connected in series. Every two AWG adjacent channels can be used to demodulate the temperature of one FBG. In this case, distributed measurements can be successfully achieved.

Experimentally, the FBG central wavelength value and its corresponding light intensity ratio algorithm are tested. The experimental results of the FBG central wavelength value and its corresponding light intensity ratio algorithm are shown in Figure 7. We then use the method of linear fitting to obtain the relationship between the light intensity ratio algorithm and the FBG central wavelength. The linear fit is used to obtain the calculated value of the FBG central wavelength. The maximum distance of the experimental point to the linear fit is 0.001 nm, i.e., the precision wavelength measurement of the system is 0.001 nm.

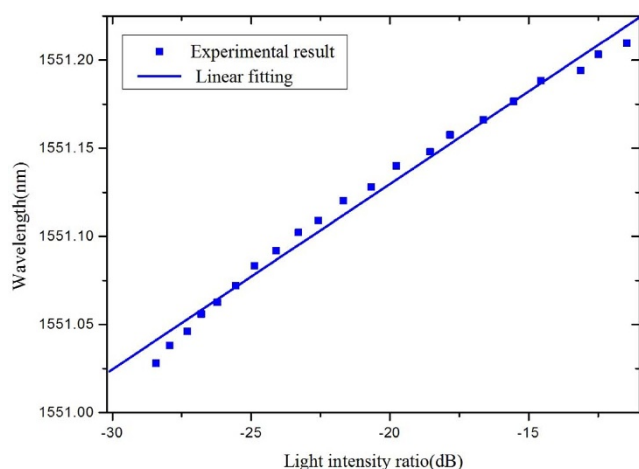


**Figure 7** | Experimental result of the FBG central wavelength value and its corresponding light intensity ratio algorithm.

In this study, an AWG demodulation integration microsystem is presented. The InP-based C-band on-chip LED has high radiant power and a wide bandwidth. The SOI-based MMI coupler has the advantages of low excess loss and a wide bandwidth. The  $1 \times 8$  AWG with a 0.4- $\mu\text{m}$ -wide waveguide exhibits low central channel loss, low non-uniformity insertion loss, low non-uniformity of the 1 and 3 dB bandwidths, and a low crosstalk level under the conditions of the same waveguide, thickness, and size. The PD has low dark current, high sensitivity, and a relatively large photosensitive area. The entire system is preliminarily tested. The precision of the wavelength measurement of the system is 0.001 nm. The wavelength sensitivity of each FBG is between 0.04 and 0.06 nm/dB. The experimental results show that this temperature demodulation system has a good linear relationship.

## Methods

InP-based LEDs and photodetectors are bonded to the SOI wafer using BCB glue. A BCB layer was spin-coated onto the upper portion of the grating coupler and was used to bond InP-based LED and photodetectors. In this case, a silica-based hybrid-integrated LED and light detector were made by adaptive grating coupling. The steps are as follows. Clean the SOI wafer. Clean and dry the InP wafer. Soft-bake the SOI wafer for 10 minutes at 100°C to remove the remaining water from the wafer. Use the spin coater to spin-coat the BCB glue onto the SOI wafer. Pre-cure process the BCB glue by soft-baking the SOI wafer spin-coated with BCB glue for 10 minutes at 150°C to remove the residual solvents and other organic impurities in the glue. Pre-bond the SOI wafer spin-coated with pre-cured BCB glue and the InP wafer. In a nitrogen atmosphere, increase the temperature of the bond tool to 250°C with a duration time of 1 hour while applying a force of 300 kPa to the wafer stack. Release the forced bond, and cool down the apparatus. The entire system is preliminarily tested as follows: Insert the FBG into the beaker with thermometer in it and then insert the AWG adjacent dual channel into the power meter. When the value of the thermometer changes, record the corresponding AWG adjacent dual channel output light intensity. Calculate the light intensity ratio logarithm and plot the curve with the method of least square method. The true experimental result is different from the fitting curve which called “noise”. The maximum distance of the experimental point to the fitting linear is the precision of the wavelength measurement of the system.

The center wavelength of the FBG’s reflection spectrum is affected by temperature and stress. The principle of demodulation is described as follows.

In the AWG demodulation integration microsystem, the AWG’s  $i$  ( $i = 1, 2, \dots, 8$ ) channel transmission spectral function can be written as

$$T_{AWG}(i, \lambda) = T_i \exp \left[ -4 \ln 2 \frac{(\lambda - \lambda_i)^2}{\Delta \lambda_i^2} \right] \quad (2)$$

where  $T_i$  is the transmission spectrum normalization factor,  $\lambda_i$  is the central wavelength of the  $i^{\text{th}}$  channel, and  $\Delta \lambda_i$  is the half-peak bandwidth of the AWG’s Gaussian spectrum.

The FBG reflection spectrum is Gaussian in nature, and its spectral function can be written as

$$R_{FBG}(\lambda) = R_0 \exp \left[ -4 \ln 2 \frac{(\lambda - \lambda_{FBG})^2}{\Delta \lambda_B^2} \right] \quad (3)$$

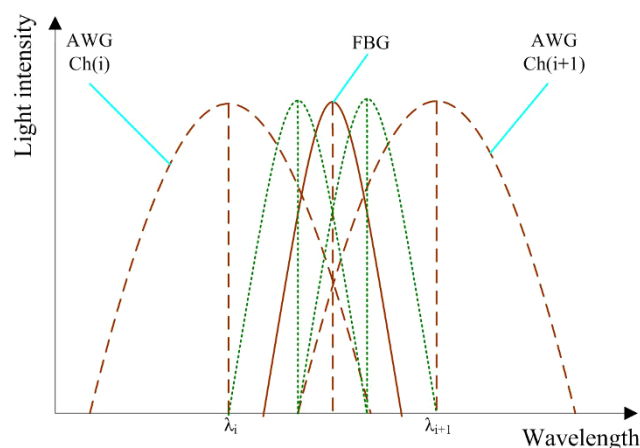


**Figure 8** | FBG reflection spectrum and AWG adjacent channel transmission spectrum at different temperatures.



In Eq. (3),  $R_0$  represents the normalization factor of the reflection spectrum,  $\lambda_{FBG}$  is the FBG's central wavelength, and  $\Delta\lambda_{FBG}$  is the half-peak bandwidth of the FBG's Gaussian spectrum. Figure 8 shows the FBG's reflection spectrum and the AWG's adjacent channel transmission spectrum under different temperatures.

When the reflected light from the FBG penetrates the AWG, light with a different wavelength separates and travels to different adjacent array waveguides. When each FBG's reflection spectrum passes through the adjacent channel of the AWG, it overlaps with the transmission spectrum of two AWG adjacent channels.  $P_i$  and  $P_{i+1}$  are the output light intensity of the AWG's two adjacent channels. In addition,  $P_i$  and  $P_{i+1}$  are the convolution of the FBG's reflection spectrum and the AWG's adjacent channel transmission spectrum, respectively. The expressions of  $P_i$  and  $P_{i+1}$  can be written as

$$P_i = (1 - L_i) \int_0^{\infty} S(\lambda) \cdot R_{FBG}(\lambda) \cdot T_{AWG}(i, \lambda) d\lambda \quad (4)$$

$$P_{i+1} = (1 - L_{i+1}) \int_0^{\infty} S(\lambda) \cdot R_{FBG}(\lambda) \cdot T_{AWG}(i+1, \lambda) d\lambda \quad (5)$$

In Eqs. (4) and (5),  $S(\lambda)$  is the output power spectrum of the light source, with the assumption that the output power is constant ( $S_0$ ) within the AWG bandwidth, and  $L_i$  and  $L_{i+1}$  are the light attenuation coefficients.  $R_{FBG}(\lambda)$  is the reflection spectrum function of sensory grating,  $T_{AWG}(i, \lambda)$  and  $T_{AWG}(i+1, \lambda)$  are the AWG channels, and  $i$  and  $i+1$  are transmission spectrum functions in the fiber grating demodulation system.

In a case in which every channel of the AWG has the same transmission coefficient and half-peak bandwidth, the relationship between the logarithm of the adjacent channel light intensity ratio of the AWG and of the FBG's central wavelength can be written as follows:

$$10 \lg \left( \frac{P_{i+1}}{P_i} \right) = 10 \times \frac{\left( \frac{8(\ln 2)\Delta\lambda}{\Delta\lambda_i^2 + \Delta\lambda_{FBG}^2} \lambda_{FBG} - \frac{4(\ln 2)(\lambda_{i+1}^2 - \lambda_i^2)}{\Delta\lambda_i^2 + \Delta\lambda_{FBG}^2} \right)}{\ln 10} \quad (6)$$

Using Eq. (6), we can obtain the wavelength of the FBG. In addition, the temperature detected by the FBG also has a linear relationship with the FBG central wavelength; therefore, the temperature can be detected using this experimental method to obtain the fitting curve for Eq. (6).

- Zhao, Y. & Liao, Y. Discrimination methods and demodulation techniques for fiber Bragg grating sensors. *Optics and Lasers in Eng.* **41**, 1–18 (2004).
- Liang, W. *et al.* Highly sensitive fiber Bragg grating refractive index sensors. *Appl. Phys. Lett.* **86**, 151122–151123 (2005).
- Huang, C. *et al.* Demodulation of fiber Bragg grating sensor using Cross-Correlation algorithm. *IEEE Photon. Technol. Lett.* **19**, 707–709 (2007).
- Willshire, A. J., Dziuda, L. & McDonald, J. R. Performance analysis of the fiber Bragg grating interrogation system based on an arrayed waveguide grating. *IEEE T. Instrum. Meas.* **53**, 1192–1196 (2004).

- Xiao, G. Z. *et al.* Interrogating fiber Bragg grating sensors by thermally scanning a demultiplexer based on arrayed waveguide gratings. *Opt. Lett.* **29**, 2222–2224 (2004).
- Bogaerts, W. *et al.* Basic structures for photonic integrated circuits in Silicon-on-insulator. *Opt. Express* **12**, 1583–1591 (2004).
- Van, C. J. *et al.* Electrically pumped InP-based microdisk lasers integrated with a nanophotonic silicon-on-insulator waveguide circuit. *Opt. Express* **15**, 6744–6749 (2007).
- Le, T. & Cahill, L. W. The design of  $4 \times 4$  multimode interference coupler based microring resonators on an SOI platform. *J. Telecommun. Inform. Technol.* **2**, 58–62 (2009).
- Zhao, L. *et al.* Design and fabrication of an 8 channel, and 1.6 nm arrayed waveguide grating based on Si nanowires. *J. Optoelectron. Laser* **21**, 1589–1592 (2010).
- Roelkens, G. *et al.* Laser emission and photodetection in an InP/InGaAsP layer integrated on and coupled to a silicon-on-insulator waveguide circuit. *Opt. Express* **14**, 8154–8159 (2006).
- Chen, H. L., Chou, Y. I. & Chu, C. Y. A novel high-sensitive Pd/InP hydrogen sensor fabricated by electroless plating. *Sensors and Actuators B: Chemical.* **85**, 10–18 (2002).

## Acknowledgements

This study is supported by the National Natural Science Foundation of China (No. 61177078, 61307094, 31271871), the Specialized Research Fund for the Doctoral Program of Higher Education of China (No. 20101201120001), and Tianjin Research Program of Application Foundation and Advanced Technology (No. 13JCYBJC16800).

## Author contributions

H.Q.L., C.Y.M., M.L.Z. and E.B.L. conceived of this study, and participated in its design. W.Q.Z., Y.L., X.Y.D., C.Z. and C.X.T. performed the experiments and revised it for scientific content. All authors read and approved the final manuscript.

## Additional information

**Competing financial interests:** The authors declare no competing financial interests.

**How to cite this article:** Li, H.Q. *et al.* Preliminary Investigation of an SOI-based Arrayed Waveguide Grating Demodulation Integration Microsystem. *Sci. Rep.* **4**, 4848; DOI:10.1038/srep04848 (2014).



This work is licensed under a Creative Commons Attribution-NonCommercial-ShareAlike 3.0 Unported License. The images in this article are included in the article's Creative Commons license, unless indicated otherwise in the image credit; if the image is not included under the Creative Commons license, users will need to obtain permission from the license holder in order to reproduce the image. To view a copy of this license, visit <http://creativecommons.org/licenses/by-nc-sa/3.0/>